Revista Argentina de Clínica Psicológica
2020, Vol. XXIX, N°4, 579-589
DOI: 10.24205/03276716.2020.863

Convergence and Stability of a Fractional Differential System in Image Processing

Yingfu Cai[a], Xiaoyang Yu[b]*

Abstract

The Perona-Malik differential equation (PMDE) is an important model in image processing. In this paper, we present a numerical scheme for the fractional form of anisotropic nonlinear PMDE with initial-boundary conditions. The stability and convergence of this scheme is verified. Finally, some numerical experiments are given for denoising, enhancing and blurring the images.

Keywords: Fractional system, Perona-Malik equation, convergence, stability, image processing

1. Introduction

The history of fractional calculus began in 1695 by Leibniz. At present, the fractional calculations are used for many applications especially in the processing of digital images and signals (see [22]-[25] and [34]). In 1997, Dobson et al. analyzed the convergence of an iterative method for problems such as total variation denoising [10]. In 1999, Kornprobst et al. [15] proposed a suitable numerical scheme based on half quadratic minimization for the problem of restoring and motion segmenting noisy image sequences with a static background, and they demonstrated its convergence and stability. In 2011 in the conference of Germany, Mastroianni et al. demonstrated the image processing method to investigate performance and stability [6]. In 2011, Liu et al.[18] proposed two new implicit numerical methods for the fractional cable equation. Moreover, they investigated the stability and convergence of these methods. In total variation denoising, one attempts to remove noise from a signal or image by solving a nonlinear minimization problem involving a total variation criterion. Several approaches based on this idea have recently been shown to be very effective, particularly for denoising functions with discontinuities. In image processing, fractional calculus is exploited in image denoising using the diffusion equation [1,7,28,31].

Enhancing contrast and preserving edges are fundamental operations in noise reduction. However, at one time, providing enhanced contrast and noise reduction is difficult. Chen et al. proposed two novel models for simultaneous image denoising and contrast enhancement using Partial Difference Equation (PDE) variational approach [9]. Models based on PDEs and calculus of variations are also generalized for fractional derivatives. For instance, fractional-order PDEs are applicable for multi-scale nonlocal contrast enhancement with texture preserving [26] and iterative learning control with high-order internal models [19]. We aim to present a numerical scheme for the fractional form of Perona-Malik formulation. Also, we investigate the stability and convergence of this numerical scheme and apply it for denoising, enhancing and blurring the images

2. Perona-Malik Formulation

Although the conventional image denoising approaches such as averaging filter or Gaussian filter are efficient in the reduction of noise, they also have the disadvantage of blurring the edges of images [4],[5]. For this sake, some techniques based on PDE anisotropic diffusion have been developed to reduce image noise without removing significant parts of the image content, typically edges, lines or other

[a,b] College of Measurement and Control Technology and Communication Engineering, Harbin University of Science and Technology, Heilongjiang, China
**Corresponding Author: Xiaoyang Yu*
Email: pangyuan39r@126.com

important details [2],[11]. Anisotropy in diffusion means that the smoothing induced by the PDE can be favored in some directions and prevented in others.

Anisotropic diffusion was first proposed by Perona and Malik [21] to image filtering as follows:

$$\begin{cases} \frac{\partial I(x,y;t)}{\partial t} = div(d(x,y)\nabla I(x,y;t))), \\ I(x,y;0) = I_0. \end{cases} \tag{1}$$

where I_0 is the unfiltered image, and after some diffusion time t, $I(x,y;t)$ will be the filtered image. Also, the function $d(x,y)$ is called diffusion coefficient that controls the diffusion rate at any location of an image domain. If d is a constant value, (1) will be equivalent to convolving the image with a Gaussian smoothing filter (isotropic diffusion) that blurs whole of the image. The idea of anisotropic diffusion is to adaptively choose d so that an image becomes smooth whose edges are preserved. The diffusion coefficient d is generally selected to be a nonnegative monotonically decreasing function of gradient magnitude. Nonlinear diffusivity $d = g(I)$ is a function reducing as the gradient grows. The stronger the edge, the smaller g and the smoother the region, the larger g.

For instances, g can be given by

$$g(I) = \frac{1}{\sqrt{1 + c|\nabla G_\gamma * I|}},$$

or

$$g(I) = \frac{1}{1 + |\nabla I|/\lambda},$$

where $(*)$ denotes the convolution operator, G_γ is the Gaussian filter with standard derivation of γ, λ and c are constant positive values.

In fact, in nonlinear diffusion, when the smoothing depends on the current diffused image, we get a nonlinear equation for the smoothing. Finding a suitable parameter λ in the diffusion coefficient is still a challenge[27].

The fractional form of nonlinear anisotropic diffusion equation (NADE) have been studied by several researchers (see for instance [29]). In fact, an arbitrary selection of the order of derivative, allows us to control the diffusion. The fracional derivative can be applied on the dynamic term (lef hand) of (1)[7] or its right hand side[12, 32]. By Euler-Lagrange equation of a cost functional, Bai and Feng in [7] proposed to apply it for image denoising. Janev et al. [13] proposed to use of a fully fractional NADE which interpolates between the parabolic and the hyperbolic PDE and, at the same time, between the second and the fourth order PDE. In 2018, Bai and Feng [8] proposed a new approach to denoise a noisy image. They have regarded the concept of fractional derivative as one kind of high-pass filter and generalized fractional derivative for a NADE satisfying some conditions.

In this paper, we consider a fractional form of NADE such that the Grünwald-Letnikov fractional derivative is used. For a function f, it is defined by [20]

$${}^{G-L}_{\ a}D^{\alpha}_{t} f(t) = \lim_{h\to 0} \frac{1}{h^\alpha} \sum_{i=0}^{[\frac{t-a}{h}]} (-1)^i \binom{\alpha}{i} f(t-ih), \tag{2}$$

where the positive real number α is the order of derivative, $[x]$ denotes the largest integer number less than or equal to x and α_i is defined as

$$\binom{\alpha}{i} = \frac{\alpha(\alpha-1)\cdots(\alpha-i+1)}{i!}.$$

The fractional form of PMDE can be given by

$$\begin{cases} {}^{G-L}_{\ a}D^{\alpha}_{t} I(x,y;t) = div(g(I)\nabla I), & (x,y,t) \in (0,a)\times(0,b)\times(0,T) \\ I(x,y;0) = I_0; & 0<x<a, 0<y<b \\ I(0,y;t) = I(a,y;t) = 0; & 0<y<b. 0<t<T \\ I(x,0;t) = I(x,b;t) = 0; & 0<x<a. 0<t<T \end{cases} \tag{3}$$

where $0 < \alpha < 1$, ∇I denotes the gradient of I and $g(I)$ is an edge-stopping function. The function g is chosen such a way that satisfies $g(I(x,y;t)) \to 0$ as $x \to \infty$ or $y \to \infty$. This arises to stop diffusion across edges. Also, I_0 is the original image. If it does not satisfy the boundary conditions, we extend the image with a black strip on the bounary of the image.

3. Numerical Scheme

The numerical solution of NADE has been studied by several researchers. In 1998, Black et al[3] presented a floating method for the time dependent term of NADE. Moreover, they computed the magnitude of gradient at each pixel based on the difference of that pixel and mean value of the neighborhood pixels. In 2002, Keeling and Stollberger[14] proposed to use of numerical scheme based upon finite differences and single-step time stepping. Furthermore, for planar images, they have diagonally discretized the diffusion operator at the cell centroid. In 2011, Janev et al[13] suggested the Caputo fractional differential equation for time dependent term and got a Voltera integral equation of the second kind. Accordingly, they generated a sequence of numerical solution. In 2016, Zho et al[33] proposed to use a generalization of the classical Adams-Bashforth-Moulton integrator.

In order to give a numerical scheme for solving (3), at first the definition of Grünwald-Letnikov (2) can be rewritten by [30]

$$ {}^{G-L}_{0}D_t^{\alpha} I(x,y;t) = \frac{1}{\Delta t^{\alpha}} \sum_{i=0}^{[\frac{t}{\Delta t}]} (-1)^i \binom{\alpha}{i} I(x,y;t-i\Delta t) + O(\Delta t), \tag{4} $$

Now, using the central differences of first derivative in space, the PMDE at point (x_j, y_k, t_n) can be given by

$$ \begin{aligned} & \frac{1}{(\Delta t)^{\alpha}} \sum_{i=0}^{n} (-1)^i \alpha_i \; I(x_j, y_k; t_n - i\Delta t) + O(\Delta t) \\ = \; & \frac{\partial}{\partial x}\Big(g(I)\frac{\partial I}{\partial x}\Big)\Big|_{(x_j,y_k,t_n)} + \frac{\partial}{\partial y}\Big(g(I)\frac{\partial I}{\partial y}\Big)\Big|_{(x_j,y_k,t_n)} \\ = \; & \frac{1}{\Delta x}\left[g(I)\frac{\partial I}{\partial x}\Big|_{(x_j+\frac{1}{2},y_k,t_n)} - g(I)\frac{\partial I}{\partial x}\Big|_{(x_j-\frac{1}{2},y_k,t_n)}\right] + O(\Delta^2 x) \\ + \; & \frac{1}{\Delta y}\left[g(I)\frac{\partial I}{\partial y}\Big|_{(x_j,y_k+\frac{1}{2},t_n)} - g(I)\frac{\partial I}{\partial y}\Big|_{(x_j,y_k-\frac{1}{2},t_n)}\right] + O(\Delta^2 y) \\ = \; & \left[\frac{1}{\Delta x} g^n_{j+\frac{1}{2},k}\Big(\frac{I^n_{j+1,k}-I^n_{j,k}}{\Delta x} + O(\Delta^2 x)\Big) - \frac{1}{\Delta x} g^n_{j-\frac{1}{2},k}\Big(\frac{I^n_{j,k}-I^n_{j-1,k}}{\Delta x} + O(\Delta^2 x)\Big) + O(\Delta^2 x)\right] \\ + \; & \left[\frac{1}{\Delta y} g^n_{j,k+\frac{1}{2}}\Big(\frac{I^n_{j,k+1}-I^n_{j,k}}{\Delta y} + O(\Delta^2 y)\Big) - \frac{1}{\Delta y} g^n_{j,k-\frac{1}{2}}\Big(\frac{I^n_{j,k}-I^n_{j,k-1}}{\Delta y} + O(\Delta^2 y)\Big) + O(\Delta y^2)\right] \\ = \; & g^n_{j+\frac{1}{2},k}\frac{(I^n_{j+1,k}-I^n_{j,k})}{\Delta^2 x} - g^n_{j-\frac{1}{2},k}\frac{(I^n_{j,k}-I^n_{j-1,k})}{\Delta^2 x} \\ + \; & g^n_{j,k+\frac{1}{2}}\frac{(I^n_{j,k+1}-I^n_{j,k})}{\Delta^2 y} - g^n_{j,k-\frac{1}{2}}\frac{(I^n_{j,k}-I^n_{j,k-1})}{\Delta^2 y} + O(\Delta x) + O(\Delta y). \end{aligned} $$

where

$I^n_{j,k} = I(x_j, y_k; t_n), g^n_{j\pm\frac{1}{2},k} = g(I(x_j \pm \frac{\Delta x}{2}, y_k; t_n))$ in which $I(x_j \pm \frac{\Delta x}{2}, y_k; t_n) = \frac{I(x_j,y_k;t_n)+I(x_{j\pm\Delta x},y_k;t_n)}{2}$ and $g^n_{j,k\pm\frac{1}{2}} = g(I(x_j, y_k \pm \frac{\Delta y}{2}; t_n))$ in which $I(x_j, y_k \pm \frac{\Delta y}{2}; t_n) = \frac{I(x_j,y_k;t_n)+I(x_{j\pm\Delta y},y_k;t_n)}{2}$.

Then

$$ \begin{aligned} \sum_{i=0}^{n} (-1)^i \alpha_i \; I^{n-i}_{j,k} \; = \; & \frac{(\Delta t)^{\alpha}}{(\Delta x)^2}\left[g^n_{j+\frac{1}{2},k}(I^n_{j+1,k} - I^n_{j,k}) - g^n_{j-\frac{1}{2},k}(I^n_{j,k} - I^n_{j-1,k})\right] \\ + \; & \frac{(\Delta t)^{\alpha}}{(\Delta y)^2}\left[g^n_{j,k+\frac{1}{2}}(I^n_{j,k+1} - I^n_{j,k}) - g^n_{j,k-\frac{1}{2}}(I^n_{j,k} - I^n_{j,k-1})\right] \\ + \; & (\Delta t)^{\alpha}(O(\Delta x) + O(\Delta y)) + O((\Delta t)^{1+\alpha}). \end{aligned} \tag{5} $$

Let $\tilde{I}^n_{j,k}$ be an approximation of $I^n_{j,k}$ at point $(x_j, y_k; t_n)$. In view of (5), an implicit numerical scheme of (3) is given by:

$$ \begin{aligned} \sum_{i=0}^{n} (-1)^i \alpha_i \; \tilde{I}^{n-i}_{j,k} \; = \; & \frac{(\Delta t)^{\alpha}}{(\Delta x)^2}\left[g^n_{j+\frac{1}{2},k}(\tilde{I}^n_{j+1,k} - \tilde{I}^n_{j,k}) - g^n_{j-\frac{1}{2},k}(\tilde{I}^n_{j,k} - \tilde{I}^n_{j-1,k})\right] \\ + \; & \frac{(\Delta t)^{\alpha}}{(\Delta y)^2}\left[g^n_{j,k+\frac{1}{2}}(\tilde{I}^n_{j,k+1} - \tilde{I}^n_{j,k}) - g^n_{j,k-\frac{1}{2}}(\tilde{I}^n_{j,k} - \tilde{I}^n_{j,k-1})\right]. \end{aligned} \tag{6} $$

As usual, in image processing we take $\Delta x = \Delta y = 1$, therefore, the implicit difference numerical scheme, (6), is summarized as follows:

$$ \begin{aligned} \sum_{i=0}^{n} (-1)^i \alpha_i \; \tilde{I}^{n-i}_{j,k} \; = \; & (\Delta t)^{\alpha}[g^n_{j+\frac{1}{2},k}(\tilde{I}^n_{j+1,k} - \tilde{I}^n_{j,k}) - g^n_{j-\frac{1}{2},k}(\tilde{I}^n_{j,k} - \tilde{I}^n_{j-1,k}) \\ + \; & g^n_{j,k+\frac{1}{2}}(\tilde{I}^n_{j,k+1} - \tilde{I}^n_{j,k}) - g^n_{j,k-\frac{1}{2}}(\tilde{I}^n_{j,k} - \tilde{I}^n_{j,k-1})], \end{aligned} \tag{7} $$

with

$$\begin{cases} \tilde{I}^0_{j,k} = I_0(x_j, y_k; 0) & 1 \le j \le N_1, \quad 1 \le k \le N_2, .2cm \\ \tilde{I}^n_{0,k} = \tilde{I}^n_{N_1,k} = 0 & 1 \le k \le N_2, \quad n = 1,2,\cdots, .2cm \\ \tilde{I}^n_{j,0} = \tilde{I}^n_{j,N_2} = 0 & 1 \le j \le N_1 \quad n = 1,2,\cdots..2cm \end{cases} \tag{8}$$

4 Stability

The stability of a numerical approach for NADE has been studied in some literatures (see for instance[?]), however, presenting some conditions under which a numerical scheme for a fractional form of NADE is stable has been less verified. In this section, we express the conditions under which the numerical scheme (7) with initial and boundary conditions (8) is stable. To this end, assuming

$$\| \tilde{I}^n \|_\infty = \max_{\substack{1\le j\le N_1 \\ 1\le k\le N_2}} |\tilde{I}_{j,k}{}^n|,$$

we have the following theorem can be expressed: The implicit numerical scheme defined by (7)-(8) is conditionally stable with respect to the norm $\|.\|_\infty$ and

$$\| \tilde{I}^n \|_\infty \le c \| \tilde{I}^0 \|_\infty, \quad n = 0,1,2,\dots, \tag{9}$$

Where c is a constant value. Proof: First, by (7) we have:

$$\left[1 + (\Delta t)^\alpha (g^n_{j+\frac{1}{2},k} + g^n_{j-\frac{1}{2},k} + g^n_{j,k+\frac{1}{2}} + g^n_{j,k-\frac{1}{2}})\right] \tilde{I}^n_{j,k} + \sum_{i=1}^n (-1)^i \alpha_i \ \tilde{I}^{n-i}_{j,k}$$
$$= (\Delta t)^\alpha (g^n_{j+\frac{1}{2},k} \tilde{I}^n_{j+1,k} + g^n_{j-\frac{1}{2},k} \tilde{I}^n_{j-1,k} + g^n_{j,k-\frac{1}{2}} \tilde{I}^n_{j,k-1} + g^n_{j,k+\frac{1}{2}} \tilde{I}^n_{j,k+1}). \tag{10}$$

Let $g^n = \inf_{j,k}\{g^n_{j+\frac{1}{2},k} + g^n_{j-\frac{1}{2},k} + g^n_{j,k+\frac{1}{2}} + g^n_{j,k-\frac{1}{2}}\}$, $G^n = \sup_{j,k}\{g^n_{j+\frac{1}{2},k} + g^n_{j-\frac{1}{2},k} + g^n_{j,k+\frac{1}{2}} + g^n_{j,k-\frac{1}{2}}\}$ and $M = \max_{n\in\mathbb{N}}\{G^n - g^n\}$.

Now, by noting that g is non-negative, in view of (10)

$$[1 + (\Delta t)^\alpha g^n] \tilde{I}^n_{j,k} + \sum_{i=1}^n (-1)^i \alpha_i \ \tilde{I}^{n-i}_{j,k} \le (\Delta t)^\alpha G^n \| \tilde{I}^n \|_\infty. \tag{11}$$

Since, (11) satisfies for all j, k, then,

$$[1 + (\Delta t)^\alpha g^n] \| \tilde{I}^n \|_\infty + \sum_{i=1}^n (-1)^i \alpha_i \ \| \tilde{I}^{n-i} \|_\infty \le (\Delta t)^\alpha G^n \| \tilde{I}^n \|_\infty. \tag{12}$$

Thus,

$$(1 - (\Delta t)^\alpha (G^n - g^n)) \| \tilde{I}^n \|_\infty \le \sum_{i=1}^n (-1)^{i+1} \alpha_i \ \| \tilde{I}^{n-i} \|_\infty. \tag{13}$$

If $\Delta t < (\frac{1}{M})^{1/\alpha}$, then $F = 1 - M(\Delta t)^\alpha > 0$ that implies

$$\| \tilde{I}^n \|_\infty \le \frac{1}{(1-(\Delta t)^\alpha (G^n - g^n))} \sum_{i=1}^n (-1)^{i+1} \alpha_i \ \| \tilde{I}^{n-i} \|_\infty \le \frac{1}{F} \sum_{i=1}^n (-1)^{i+1} \alpha_i \ \| \tilde{I}^{n-i} \|_\infty. \tag{14}$$

By induction on n, we show that

$$\| \tilde{I}^n \|_\infty \le (\frac{1}{n} x + \sum_{i=2}^{n-1} 2^{i-2} x^i + x^n) \| \tilde{I}^0 \|_\infty , \qquad n \ge 3, \tag{15}$$

where $x = \frac{\alpha}{F}$. For $n = 1,2$ and $n = 3$, by (14) we have:

$$\begin{array}{lll} n = 1 \implies & \| \tilde{I}^1 \|_\infty & \le \frac{\alpha}{F} \| \tilde{I}^0 \|_\infty = x \| \tilde{I}^0 \|_\infty, \\ n = 2 \implies & \| \tilde{I}^2 \|_\infty & \le \frac{1}{F}(\alpha \| \tilde{I}^1 \|_\infty + \frac{\alpha(1-\alpha)}{2} \| \tilde{I}^0 \|_\infty) \le ((\frac{\alpha}{F})^2 + \frac{1}{2}(\frac{\alpha}{F})) \| \tilde{I}^0 \|_\infty \le (x^2 + \frac{1}{2}x) \| \tilde{I}^0 \|_\infty, \\ n = 3 \implies & \| \tilde{I}^3 \|_\infty & \le \frac{1}{F}(\alpha \| \tilde{I}^2 \|_\infty + \frac{\alpha(1-\alpha)}{2} \| \tilde{I}^1 \|_\infty + \frac{\alpha(1-\alpha)(2-\alpha)}{3!} \| \tilde{I}^0 \|_\infty) \\ & & \le \frac{\alpha}{F}(\| \tilde{I}^2 \|_\infty + \frac{1}{2} \| \tilde{I}^1 \|_\infty + \frac{1}{3} \| \tilde{I}^0 \|_\infty) \le ((\frac{\alpha}{F})^3 + (\frac{\alpha}{F})^2 + \frac{1}{3}(\frac{\alpha}{F})) \| \tilde{I}^0 \|_\infty \\ & & \le (x^3 + x^2 + \frac{1}{3}x) \| \tilde{I}^0 \|_\infty \le (x^3 + 2x^2 + \frac{1}{3}x) \| \tilde{I}^0 \|_\infty, \end{array}$$

(16)

that satisfies the inequality (15) for $n = 3$. Now, we assume that (15) holds for $n = 1,2,\dots,m-1$. We show that (15) satisfies for $n = m$.

$$\begin{aligned} \|\tilde{I}^m\|_\infty &\le \frac{1}{F}(\alpha\|\tilde{I}^{m-1}\|_\infty+\frac{\alpha(1-\alpha)}{2!}\|\tilde{I}^{m-2}\|_\infty+\cdots+\frac{\alpha(1-\alpha)(2-\alpha)\ldots(m-1-\alpha)}{m!}\|\tilde{I}^0\|_\infty) \\ &\le x(\|\tilde{I}^{m-1}\|_\infty+\frac{1}{2}\|\tilde{I}^{m-2}\|_\infty+\cdots+\frac{1}{m}\|\tilde{I}^0\|_\infty) \\ &\vdots \\ &\le (x^m+2^{m-3}x^{m-1}+\cdots+2x^2+\frac{1}{m}x)\|\tilde{I}^0\|_\infty. \end{aligned} \tag{17}$$

Now, if $x < 1/2$, then the geomteric series implies that

$$\sum_{i=2}^{n-1} 2^{i-2}x^i \le \sum_{i=2}^{\infty} 2^{i-2}x^i = \frac{x^2}{1-2x^2}. \tag{18}$$

Finally, in view of (15) and (18)

$$\|\tilde{I}^n\|_\infty \le \frac{x^2}{1-2x^2}\|\tilde{I}^0\|_\infty \le c\|\tilde{I}^0\|_\infty. \tag{19}$$

Theorem 1 states that the numerical scheme defined by (7)-(8) is stable if $\frac{\alpha}{F} = x < 1/2$ and $F > 0$. That is, the scheme is stable if

$$\alpha < 1/2, \qquad \Delta t < (\frac{1-2\alpha}{M})^{1/\alpha}.$$

In the given numerical scheme, if we use the derivatives such as Prewitt or Roberts instead of forward derivative, a similar result will be obtained. In fact, just the value of F will be changed such that for Prewitt operator, $F = 1 - 16M(\Delta t)^\alpha$ and for Roberts operator, $F = 1 - 12M(\Delta t)^\alpha$ will be derived.

5. Convergence

Let I be the exact solution of (8). Take $\Delta x = \Delta y = 1$, $e_{j,k}^n := I_{j,k}^n - \tilde{I}_{j,k}^n$ for $1 \le j \le N_1, 1 \le k \le N_2, n \ge 0$. It follows from (5) and (7) that

$$\begin{aligned} \sum_{i=0}^{n} (-1)^i \alpha_i \; e_{j,k}^{n-i} &= (\Delta t)^\alpha[g_{j+\frac{1}{2},k}^n(e_{j+1,k}^n - e_{j,k}^n) - g_{j-\frac{1}{2},k}^n(e_{j,k}^n - e_{j-1,k}^n)0.3cm \\ &+ g_{j,k+\frac{1}{2}}^n(e_{j,k+1}^n - e_{j,k}^n) - g_{j,k-\frac{1}{2}}^n(e_{j,k}^n - e_{j,k-1}^n)] + O((\Delta t)^\alpha). \end{aligned}$$

Then,

$$\begin{aligned} e_{j,k}^n &= -\sum_{i=1}^{n} (-1)^i \alpha_i \; e_{j,k}^{n-i} + (\Delta t)^\alpha[g_{j+\frac{1}{2},k}^n(e_{j+1,k}^n - e_{j,k}^n) - g_{j-\frac{1}{2},k}^n(e_{j,k}^n - e_{j-1,k}^n) \\ &+ g_{j,k+\frac{1}{2}}^n(e_{j,k+1}^n - e_{j,k}^n) - g_{j,k-\frac{1}{2}}^n(e_{j,k}^n - e_{j,k-1}^n)] + c((\Delta t)^\alpha), \end{aligned}$$

where $c > 1$ is a constant value. Hence, similar to the proof of Theorem 4

$$\|e^n\|_\infty \le \frac{\sum_{i=1}^{n}|\alpha_i|\,\|e^{n-i}\|_\infty + c(\Delta t)^\alpha}{1-(\Delta t)^\alpha(G^n - g^n)} \le \frac{\sum_{i=1}^{n}|\alpha_i|\,\|e^{n-i}\|_\infty + c(\Delta t)^\alpha}{1-M(\Delta t)^\alpha}. \tag{20}$$

Let $\alpha_i = |\alpha_i|$ for $i = 1,2,3,\cdots$. It is readily seen that

$$\alpha_i \le \frac{1}{i}\alpha \qquad i = 1,2,3,\cdots. \tag{21}$$

From (20) it follows that for $n = 1$,

$$\|e^1\|_\infty \le \frac{\alpha_1\|e^0\|_\infty + c(\Delta t)^\alpha}{1-M(\Delta t)^\alpha} \le \frac{C}{F}(\Delta t)^\alpha,$$

since $\frac{1}{1-M(\Delta t)^\alpha} < \frac{1}{F}$. For $n = 2$,

$$\|e^2\|_\infty \le \frac{\alpha_1\|e^1\|_\infty + \alpha_2\|e^0\|_\infty + c(\Delta t)^\alpha}{1-M(\Delta t)^\alpha} \le \frac{1}{F}(\alpha_1\frac{C}{F} + C)(\Delta t)^\alpha = \frac{C}{F}(\frac{\alpha_1}{F} + 1)(\Delta t)^\alpha.$$

For $n = 3$,

$$\begin{aligned} \|e^3\|_\infty &\le \frac{\alpha_1\|e^2\|_\infty + \alpha_2\|e^1\|_\infty + \alpha_3\|e^0\|_\infty + c(\Delta t)^\alpha)}{1-M(\Delta t)^\alpha} \\ &\le \frac{1}{F}\left[\alpha_1\frac{C}{F}(\frac{\alpha_1}{F} + 1) + \alpha_2\frac{C}{F} + C\right](\Delta t)^\alpha \\ &\le \frac{C}{F}\left[(\frac{\alpha_1}{F})^2 + 2(\frac{\alpha_1}{F}) + 1)\right](\Delta t)^\alpha. \end{aligned}$$

In the last inequality, we used the relation(21). Repeating this process implies that

$$\|e^n\|_\infty \le \frac{C}{F}\left[(\frac{\alpha}{F})^n + n(\frac{\alpha}{F})^{n-1} + (n-1)(\frac{\alpha}{F})^{n-2} + \cdots + \frac{\alpha}{F} + 1\right](\Delta t)^\alpha. \tag{22}$$

Letting $f_n(x) = \sum_{i=1}^{n} x^i$ for $0 < x < 1$ and recalling that $\lim_{n\to\infty} f_n(x) = \frac{1}{1-x}$ and $\lim_{n\to\infty} f_n'(x) = \frac{1}{(1-x)^2}$, in view of (22) it follows that

$$\| e^n \|_\infty \leq \frac{C}{F}\frac{(\Delta t)^\alpha}{(1-\frac{\alpha}{F})^2} = \frac{CF}{(F-\alpha)^2}(\Delta t)^\alpha = C^*(\Delta t)^\alpha, \tag{23}$$

where $C^* = \frac{CF}{(F-\alpha)^2}$. In (23), we used this reality that $\frac{\alpha}{F} < 1$. Thus $\| e^n \|_\infty \leq C^*(\Delta t)^\alpha$ and the scheme is convergent.

6 Numerical Experiments

In this section, we implement the given numerical scheme for Perona-Malik formulation that is applicable for denoising, enhancing a low-contrast image or deblurring a blurred image. The implicit system given by (7) is numerically solved by Jacobi iterative method. The stop criterion is thought of as $\| \tilde{I}^{n+1} - \tilde{I}^{n+1} \|_\infty \leq \epsilon$ where ϵ is an acceptable tolerance. For all examples, we considered $g(I) = 1/(1 + |\nabla I|/\lambda)$.

Example 1

Figure 1: *Denoising an image : (a) Original noisy image . The output of the scheme for diffusion coefficient of (b) $\lambda = 0.2$. (c) $\lambda = 0.1$ and $\lambda = 0.02$.*

For the first example, we consider a color image (Figure 1(a)) of size 500×500 which is a noisy image by salt and pepper noise. In order to denoise this image, we apply the numerical scheme of (7) by $\alpha = 0.4$ and $\Delta t = 0.003$. Moreover, the diffusion coefficient is considered with different values of λ. The dimension of the resulting system will be 250000×250000 for each of the red, green and blue colors. Figures (1b)-(1d) show the implementation of our Peronal-Malik scheme with diffusion parameter $\lambda = 0.2, 0.1$ and $\lambda = 0.02$, respectively. As is seen, the denoising is sensetive to the value of λ and for $\lambda = 0.2$ the best denoising is happened. That is because the gradient magnitude in diffusion coefficient $g(I)$ is used to detect an image edge or boundary as a step discontinuity in intensity. But If $\nabla I >> \lambda$, then $g(I) \to 0$, and there is no movement; If $\nabla I << \lambda$, then $g(I) \to 1$, and isotropic diffusion (Gaussian filtering) is achieved. The average of elapsed CPU time is 28 seconds for $T = 10\Delta t$.

Example 2

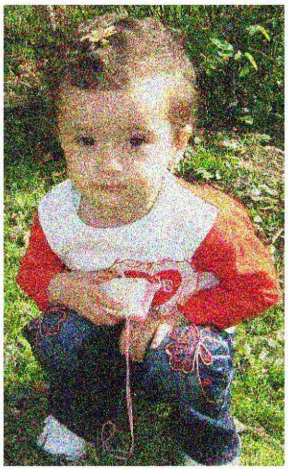

[a]

[b]

[c]

[d]

Figure 2: *Denoising a Gaussina noisy image : (a) Original Gaussinan white noise image . The output of the scheme for diffusion coefficient of (b)* $\lambda = 1$. *(c)* $\lambda = 0.2$ *and* $\lambda = 0.1$.

In the second example, we consider another color image (Figure 2(a)) of size 879×1440 which is a noisy image by Gaussian white noise with mean of zero and variance of 0.02. In order to denoise this image, we apply the numerical scheme of (7) by $\alpha = 0.4$ and $\Delta t = 0.003$. Moreover, the diffusion coefficient is considered with different values of λ. The dimension of the resulting system will be 1265760×1265760 for each of the red, green and blue colors. According to $g(I) = 1/(1 + |\nabla I|/\lambda)$, as λ tends to zero, the amount of $|\nabla I|$ will be less effective and $g(I)$ will tend to zero. This means that for a very small value of λ, there is only a small change in the image. On the other hand, as λ tends to 1, the magnitude of $|\nabla I|$ will be more effective. Therefore, as λ tends to 1, we expect smoothness in the edges. Thus, for $\lambda = 1$, a better result is expected. Figures (2b)-(2d) show the implementation of our Peronal-Malik scheme with diffusion parameter $\lambda = 1{,}0.2$ and $\lambda = 0.1$, respectively. As is observed, for $\lambda = 1$ the best denoising is happened.

Example 3

[a]

[b]

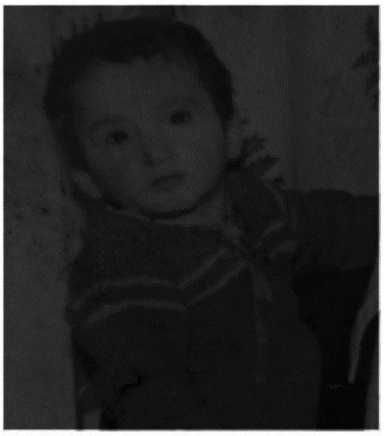

[c]

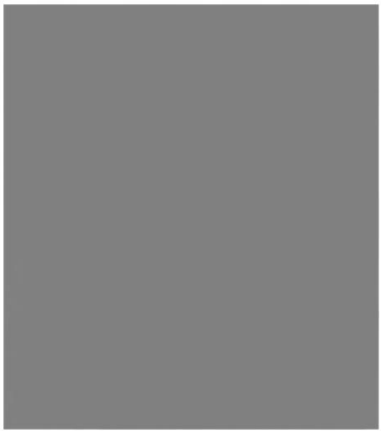

[d]

Figure 3: *Comparison of the given numerical scheme for Perona-Malik equation: (a) Original image. (b) The output of the scheme for $\alpha = 0.4$. (c) $\alpha = 0.8$ and $\alpha = 1$.*

For the third example, we consider the low-contrast image (3) of size 686×773 and present a comparison of the sharpening the image with the numerical scheme of Perona-Malik fractional differential equation (PMFDE) (7) with the conditions given in (8). We let $M = 2$ and $\Delta t = 0.003$ satisfying the stability condition for $\alpha = 0.4$. We use the Jacobi iteration method to solve the given system in the scheme. The dimension of this system is 530278×530278. The Figures (3), (3) and (3) show the implementation of sharpening algorithm for $\alpha = 0.4,0.8$ and 1, respectively. Let I and $\tilde{I}$ be the original image and the image given by the numerical scheme (7) , respectively. The steps of sharpening algorithm are as follows:

1. $g_{mask} = I - \tilde{I}$;
2. $\bar{I} = I + g_{mask}$.

Here, $\bar{I}$ is the output of the algorithm. As is seen, the lower α , the better sharpening. For $\alpha = 0.4$, a better enhancement is observed and for $\alpha = 1$, the image has very low contrast.

Example 4 *For the fourth example, we consider the Figure of "Lena" (Figure 4) of size 512×512 , therefore, the dimension of the resulting syetem will be 262144×262144. The aim is to blur the right eye of "Lena" (Figure 4) by the numerical scheme (7). Based on (7), when α decreases, the value of $I_{j,k}^n$ deceases and so we expect a dark blurring as α deacreases. Figures 3(b)-3(d) show the implementation of our scheme for $\alpha = 0.6,0.8$ and $\alpha = 1$. It is observed that as the order of fractional derivative α increases, the blurring would be lighter.*

For all cases, the diffusion coefficient $\lambda = 0.2$ has been selected.

Figure 4: *(a) The original image of Lena. Applying the numerical scheme based on PMFDE for blurring the right eye of Lena for (b) $\alpha = 0.6$ (c) $\alpha = 0.8$ and (d) $\alpha = 1$.*

Example 5 For the last example, CT scan of a human head is considered in Figure 5 of size 512×512, that implies the dimension of 262144×262144 for the resulting syetem. Our aim is to blur whole of the image. Figures 5-5 show the implementation of the given numerical scheme with $\alpha = 0.4, 0.3$ and $\alpha = 0.2$, respectively. For all cases, $\Delta t = 0.003$ is considered. It is observed that as the fractional order α decreases, the measure of blurring increases. It is obviously concluded based on the relation (7).

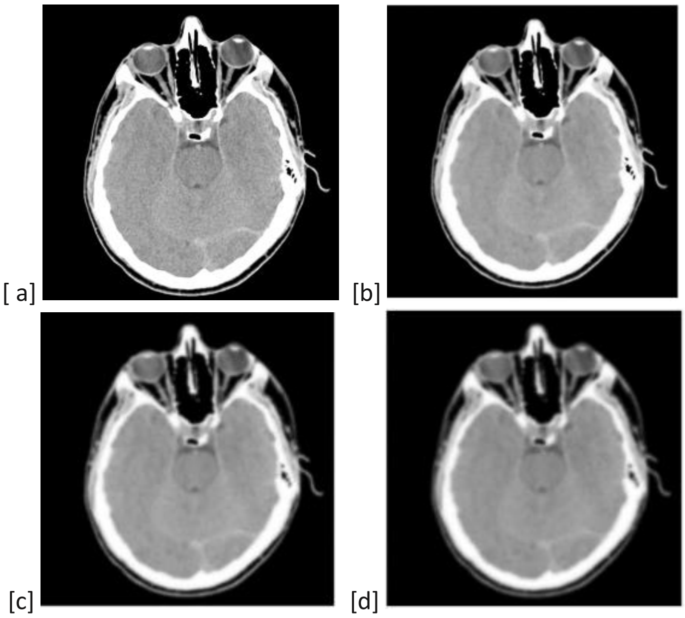

Figure 5: *(a) CT scan of a human head, and applying the numerical scheme on PMFDE for blurring the CT scan with (b) $\alpha = 0.4$, (c) $\alpha = 0.3$ and (d) $\alpha = 0.2$.*

7. Conclusion

In this paper, we have presented a numerical scheme for a fractional-order nonlinear anisotropic diffusion based on Perona-Malik PDE. This scheme is applicable for denoising a noisy image and enhancing a low-contrast image. We have proved that the scheme is convergence and conditionally stable.

References

Abrirami A, Prakesh P, Thangavel PK. Fractional diffusion equation-based image denoising model using CN-GL scheme. Int J Comput Math., 2018; 95(6-7): 1222–1239.

Alvarez L. Images and PDE's. Proceedings of ICAOS '96., Lecture Notes in Control and Information Sciences. 1996; 219:3-14.

Black MJ, Sapiro G, Marimont DH, Hegger D. Robust Anisotropic Diffusion. IEEE Trans. Image Processing. 1998; 7(3): 421–432.

Gonzales R., Woods R. Digital Image Processing. 4th ed. New York: Prentice Hall; 2018.

Jain, AK. Fundamentals of Digital Image Processing. New Jersey: Prentice Hall, USA; 1989.

Asghar M, Miettunen M, Mastroianni S, Halme J, Lund P. Demonstration of image processing method to investigate performance and stability. 26th European Photovoltaic Solar Energy Conference, Hamburg, Germany. 2011; 563–566.

Bai J, Feng XC. Fractional-order anisotropic diffusion for image denoising. IEEE Trans Image Process. 2007; 16(10): 2492–2502.

Bai J, Feng XC, Image denoising using generalized anisotropic diffusion, J Math Imag Vision. 2018; 60: 994–1007.

Chen Y, Yu Q. A partial differential equation variation approach for simultaneous image denoising and contrast enhancement. IEEE International Conference on Computer and Communications (ICCC). 2015; DOI: 10.1109/CompComm.2015.7387551.

Dobson DC, Vogel CR. Convergence of an iterative method for total variation denoising, SIAM J Numer Anal. 1997; 5(34): 1779–1791.

Guichard F, Moisan L, Morel JM. A review of P.D.E. models in image processing and image analysis, Journal de Physique 2001; 4: 137-154.

Hu S, Liao Z, Chen W. Sinogram restoration for lowdosed X-ray computed tomography using fractional-order Perona-Malik diffusion. Mathematical Problems in Engineering. 2012, Article ID 391050, 13 pages.

Janev M, Pilipovic S, Atanacković T, Obradović R, Ralevic N, Fully fractional anisotropic diffusion for image denoising, Math Comput Modelling, 2011; 54 (1-2), 729-741.

Keeling S L, Stollberger R. Nonlinear anisotropic diffusion filtering for multiscale edge enhancement. Inverse Probl. 2002, 18: 175-190.

Kornprobst P, Deriche R, Aubert G. Image sequence analysis via partial differential equation, J Math Imaging Vis. 1999; 11: 5–26.

Li L, Gao H. The stabilizability of heat equations with time-dependent coefficients. Math Meth Appl Sci. 2019;1-9.

Li L, Xu D. Alternating direction implicit-Euler method for the two-dimensional fractional evolution equation. J Comput Phys. 2013; 236: 157–168.

Liu F, Yang Q, Turner I. Two new implicit numerical methods for the fractional cable equation, J Comput Nonlin Dyn.2011; 6(1): 1–7.

Liu Sh, Wang J, Analysis of iterative learning control with high-order internal models for fractional differential equations, J Vib Control. 2018; 24(6): 1145–1161.

Podlubny I. Fractional Differential Equations. 1999: Academic Press. New York.

P. Perona, and J. Malik, Scale-space and edge detection using anisotropic diffusion, IEEE Trans. Pattern Analysis and Machine Intelligence, 1990; 12, 629-639.

Pu YF. Analog Circuit Realization of Arbitrary-Order Fractional Hopfield Neural Networks: A Novel Application of Fractor to Defense against Chip Cloning Attacks. IEEE Access. 2016; 4: 5417–5435.

Pu YF. Fractional-Order Euler-Lagrange Equation for Fractional-Order Variational Method: A Necessary Condition for Fractional-Order Fixed Boundary Optimization Problems in Signal Processing and Image Processing. IEEE Access. 2016; 4; 10110–10135.

Pu YF, Yi Z, Zhou JL. Defense against Chip Cloning Attacks Based on Fractional Hopfield Neural Networks. Int J Neural Syst. 2016; 27(4): 1–28.

Pu YF. Measurement Units and Physical Dimensions of Fractance-Part I: Position of Purely Ideal Fractor in Chuas Axiomatic Circuit Element System and Fractional-Order Reactance of Fractor in Its Natural Implementation. IEEE Access.2016; 4: 3379–3397.

Pu YF, Siarry P, Chatterjee A, Wang ZN, Yi Z, Liu Y, Zhou J, Wang Y. A Fractional-order variational framework for retinex: fractional-order partial differential equation-based formulation for multi-scale nonlocal contrast enhancement with texture preserving, IEEE T Image Process. 2018: 27(3); 1214–1229.

Tsiotsios C, Petrou M. On the choice of the parameters for anisotropic diffusion in image processing. Pattern Recognit. 2013; 46: 1369-1381.

Verma AK, Saini BS. Forward-backward processing technique for image denoising using FDZP 2D filter, J Appl Res Technol. 2018: 15; 538–592.

Wang Y, Shao Y, Gui Z, Zhang Q, Yao L, Liu Y, A Novel Fractional-Order Differentiation Model for Low-Dose CT Image Processing, IEEE Access, 2016: 4; 8487-8499.

Yuste SB, Acedo L. An explicit finite difference method and a new Von Neumann-type stability analysis for fractional diffuion equations, SIAM J Numer Anal. 2005: 42(5); 1862-1874.

Zhang W, Li J, Yang Y. A fractional diffusion-wave equation with non-local regularization for image denoising, Signal Process. 2014; 103: 6–15.

Zhang YS, Zhang F, Li BZ. Image restoration method based on fractional variable-order differential. Multidimens. Syst. Signal Process. 2018: 29; 999-1024.

Zhou Q, Gao J, Wang Z, Li K. Adaptive Variable Time Fractional Anisotropic Diffusion Filtering for Seismic Data Noise Attenuation. IEEE Trans. Geoscience and Remote Sensing. 2016; 54(4): 1905–1917.

Zhu P, Xiang Q. Oscillation criteria for a class of fractional delay differential equations, Adv Differ Equ-ny. 2018; doi.org/10.1186/s13662-018-1813-6.